Large-area, polarisation-sensitive, plasmonic materials from colloidal lithography

Anthony John Morfa [*,1], Valerio Oddone[,1], and Michael Giersig[1, 2]**

[1] Department of Physics, Freie Universität Berlin, Arnimallee 14, 14195 Berlin, Germany
[2] Helmholtz-Zentrum Berlin für Materialien und Energie, Hahn-Meitner-Platz 1, 14109 Berlin, Germany

Keywords Plasmonics, polarization, nanosphere lithography, self-assembly.

* Corresponding author: e-mail Anthony.Morfa@kit.edu, Phone: +49 6221 - 54 19 122
** e-mail valerio.oddone@gmail.com, Phone: +49 838 54294

The development of simple to prepare, polarization-sensitive plasmonic apertures with two plasmonic modes, is described. To achieve these results, monocrystalline nanosphere lithography masks of 438 nm polystyrene spheres are modified with reactive ion etching before silver is subsequently evaporated through the mask at varied angles. As the angle of evaporation increases, round apertures, elliptical apertures or lines with bow-tie like features between two lines are produced. A primary plasmon mode is shown at 570 nm, while a tunable plasmon mode is demonstrated between 700 and 900 nm. Finite-difference time-domain calculations agree with the observed results and predict that this method of fabrication can produce tunable plasmonic features throughout the NIR optical telecommunication wavelength range. Lastly, the excitation polarization angle is compared with that of plasmonic nanorods and asymmetric nano-apertures systems to describe why the excitation polarization of the low energy mode is orthogonal to the long axis of the apertures.

1 Introduction Surface plasmon active materials have been utilized in a number of applications, for instance for enhanced spectroscopic methods [1, 2], sensing platforms [3-5], and enhanced energy conversion [6-9] (to name just a few). Several other applications are expected to benefit from surface plasmon active materials, but require both wavelength and polarization control of the surface plasmon resonance to be realized [10-12]. To date, the strong local electric fields near a metal surface and the corresponding sensitivity to the surrounding dielectric media of localized surface plasmons have been generated on a number of different surfaces. Examples range from roughened metal electrodes [13] to lithographically produced apertures [14] and nanometre-scaled objects [15], and, of course, nanoparticles [16, 17]. Tunability of the surface plasmon frequency using current methods for fabrication largely relies on preparing a new lithographic mask or synthesizing new nanoparticles for each desired plasmon resonance [18].

Nanosphere lithography (NSL) is one popular method for producing surface plasmon active materials due to its low fabrication cost and the large size of the sample area produced (as large as 50-200 cm²) [18-20]. Though modification of the nanosphere layer can lead to tunable optical transmission; changing the plasmon resonance frequency relies on changing the initial sphere size. Several specialized methods have been demonstrated to prepare complex morphologies with controllable optical properties from nanosphere lithography masks, but these methods require metal evaporation chambers with specialized sample stages, custom geometries and at least two axis of rotation to be realized [21-23]. We describe herein a method fabricate plasmonic structures through which it is possible to tune the plasmon resonance frequency by changing the optical polarization angle. Said structures are achieved through controlled evaporation in a custom-built evaporation chamber with only a single tilt axis.

Recent interest in polarization sensitive plasmonic structures has been driven by potential applications in HDTV11 and telecommunication technologies [12] and has largely been undertaken on perforated silver films prepared with electron beam lithography. The high degree of control over these surfaces enables very precise aperture dimensions and shapes, but typically on a very small size scale. This has been ideal for understanding the role physical structure plays in controlling how the plasmon resonance interacts with polarized light, but does not represent

an easy method for preparing the large area structures required for the proposed applications [24-26].

1.1 Nanosphere Lithography We have developed structures from simple to prepare NSL masks with wavelength tunable and polarization sensitive optical properties.

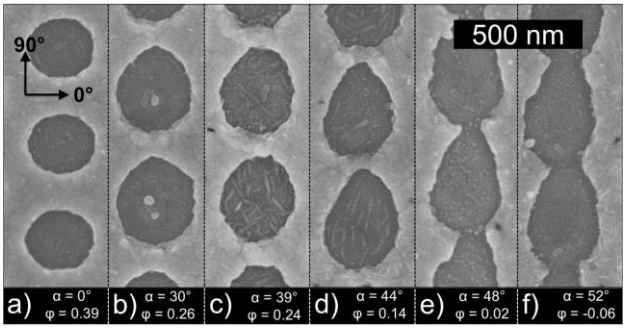

Figure 1 SEM micrographs of representative 50 nm silver films on glass as a function of silver deposition angle. The calculated value of $\varphi = ((R_o-R_i)/R_o)$ is shown for each deposition angle. The polarization angle for incident light for subsequent figures is marked in the left most panel. For all images, the periodicity corresponds to the original sphere size of 438 nm, the width of the holes to the etched sphere size of 270 nm ± 10 nm.

Typically, NSL utilizes a hexagonally close-packed array of nano- or microspheres on a surface as an evaporation mask. Without modification, a hexagonal array of triangular prisms is produced via metal deposition. By reducing the sphere size first, a hexagonal array of apertures in the deposited metal is produced. Additional structures can be fabricated if large, monocrystalline NSL masks are first produced and then oriented with respect to the metal evaporation source before metal deposition. In this paper, we demonstrate that, by changing the angle of metal evaporation through the lithographic mask, the shape of the aperture can be tuned from circular to elliptical apertures and eventually lines. Unlike previous techniques, such as the so-called angle-resolved NSL (AR-NSL) [23], the nanosphere is reduced in size before metal evaporation, and unlike the so-called shallow-angle NSL (SANSL) [21] the angle of deposition is controlled for aperture ellipticity, not line formation. In this way, a fast and easy production of macroscopic arrays of oriented anisotropic nanostructures is demonstrated, with control of the geometry that is unusual for self-assembled techniques. For mass production, this method can be transferred to other lithographic methods and is expected to be broadly applicable to interference lithography or nanoindent or stamp-based lithographies for large-scale fabrication.

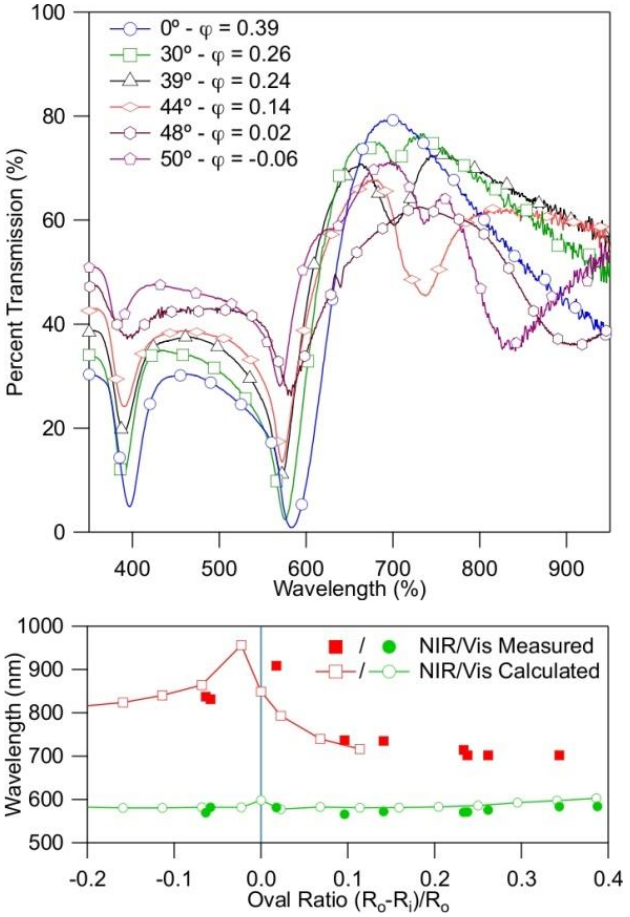

Figure 2 Measured optical transmission spectra for 50 nm silver films on glass, at normal incidence and for unpolarized light (top). Measured transmission minima (from top) for both the high frequency (Vis) and low frequency (NIR) plasmon absorption features as a function of the ratio $\varphi = ((R_o-R_i)/R_o)$ (as seen in Fig. 1).

2. Experimental In the scanning electron microscopy (SEM - obtained on a Hitachi SU8030) data shown in Fig. 1, a series of perforated silver films (50 nm silver on a 2 nm titanium adhesion layer) is shown. The silver films were produced by evaporating silver through 438 nm diameter polystyrene spheres (purchased from Microparticles GmbH), reduced to a diameter of 270 nm by etching the surface for 350 s, at a plasma power of 64 W and gas flow of 1 sccm O_2 at 0.06 mbar in a (plasma technologies GmbH "MiniFlecto") oxygen plasma system. As the angle of silver deposition is changed between 0 and 52 degrees (defined as the angle between the sample normal and the direction of evaporation), round apertures, then elliptical apertures and finally linear rows of silver lines dotted with bow-tie-like features are produced. In Fig. 1, the ratio φ, is defined as $(R_o-R_i)/R_o$ (Where R_o is the initial radius (219 nm) of the non etched spheres, i.e. the distance between the holes, and R_i the measured semimajor axis of the ellipse), leading to connected holes for negative φ. In order to align the grating vector of the two-dimensional array of spheres with the angle of metal deposition, the array orientation is

first mapped via bright field optical microscopy on a purpose built stage (see Supplementary Information 1) [27]. The stage can then be rotated to the correct angle before metal deposition to enable the formation of elliptical apertures with long axis in the direction of the grating vector. For this study, crystalline regions (with 2D crystal axis varying no more than ± 2°) of few cm² were produced (see Supplemental Information 1). As has been shown in previous work, depending on the size and quality of the spheres, as well as on the method of fabrication, crystals of over 50 cm² can be achieved [18]. The spacing between two metal rows and the critical angle where the transition between the sphere-ellipse-line takes place is determined by the etched sphere size and the corresponding geometry of the system (in the present case the average aperture short axis is 270 nm, which is also the distance between wires, and the critical angle where the array of apertures becomes an array of lines is ~ 48º).

The transmission of the produced nanostructures was measured with polarization dependency in a *Thermo Scientific Evolution Array* UV/Vis spectrometer.

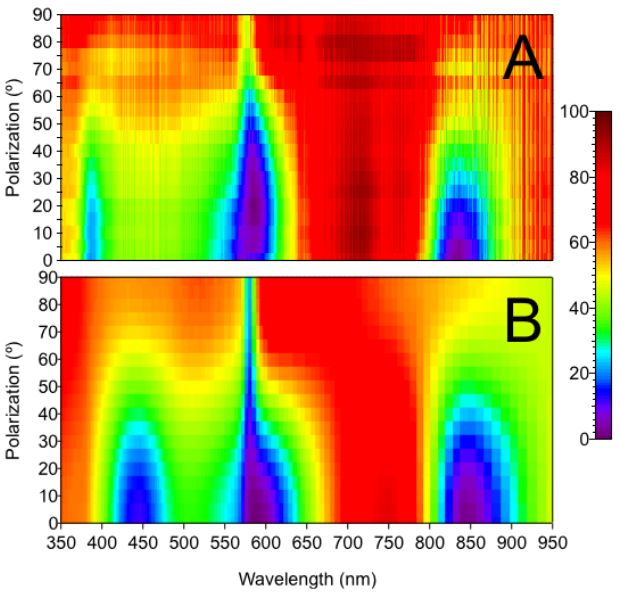

Figure 3 Measured (a) and calculated (b) optical transmission spectra as a function of wavelength and polarization angle through a 50 nm silver film on glass, as shown in Fig. 1

3 Results and discussion The effect of elongating the aperture on the optical properties of the perforated film is twofold. First, as can be seen in Fig. 2 (top), once the length of the ellipse approaches the period of the array, a second resonance appears at lower energies than the primary resonance. For apertures produced from 438 nm polystyrene spheres, the primary plasmonic feature is at 570 nm while the second, higher wavelength appears between 700 nm and 910 nm. This second resonance is sensitive to the dimensions of the ellipsoid and shifts nearly 210 nm in wavelength with changing ellipticity of the apertures (see Fig. 2 (bottom)). In general, the excitation wavelengths of both plasmon modes are in excellent agreement with finite-difference time-domain calculations. Interestingly, the primary resonance associated with hexagonally close-packed arrays of apertures remains nearly constant throughout the transition from circular apertures to elliptical apertures and finally to linear rows dotted with bow-tie-like features.

The second effect is that, where, for round holes, there was no difference in optical properties with polarization (see Supplementary Information 2) [27], for the elliptical hole-array as the length of the ellipse approaches the period of the array, new features appear, and as the ellipsoids become longer than the period of the array, i.e. 'percolating' into continuous apertures, the feature shows strong polarization sensitivity (see Fig. 3). When the polarization of the incident light is perpendicular to the long axis of the ellipsoids (0° in Fig. 3), the low energy plasmon is excited and leads to both plasmonic features being observed. When the polarization is rotated by 90° to be parallel to the long axis of the ellipsoids, only the initial high-energy plasmon resonance remains, even though less marked. For hexagonally close-packed apertures, the spectral location of a plasmon resonance can be approximated by equation 1 (where '*a*' is the original nanosphere diameter or grating period, *i* and *j* the scattering orders of the array, ε_m and ε_d the permittivity of the metal and of the dielectric in contact with the metal) [10]. Applying equation 1 to the samples presented in Fig. 1 and 2, it is expected that as the incident polarization is rotated, weak maxima and minima in the plasmonic features will appear at 60-degree intervals. However, for such samples, where the grating spacing and aperture diameter are similar, we find a distinct lack of polarization sensitivity (see Supplemental Information 2). More importantly, the same equation cannot explain the frequency, nor the excitation polarization of the low-frequency mode present once the elliptical long axis is longer than the grating period [24].

$$\lambda_{SP} = \frac{a}{\sqrt{4/3(i^2+ij+j^2)}} \cdot \sqrt{\frac{\varepsilon_m \varepsilon_d}{\varepsilon_m+\varepsilon_d}} \qquad (1)$$

For rectangular apertures, similar observations as the low-frequency plasmonic resonances seen herein were attributed to localized surface plasmon modes [25]. For these modes, it is useful to compare the surface plasmon modes and the corresponding polarization of excitation to nanorods of the same plasmonic metal. For rectangular apertures, the modes excited by polarized light are geometrically orthogonal to those of the nanorods, with the low frequency mode excited along the short axis of the aperture and the high frequency mode excited along the long axis of the aperture. Initially, this difference was simply described by the "complementarity between holes and particles" [25] and was subsequently described using a quasi-static model by Sepúlveda et al [26]. In the present case, where the

strong polarization dependence is seen once the elliptical long axis is longer than the grating spacing, there is no simple complementarity to this geometry. However, the resulting structure is reminiscent of bow-tie antennae spaced out evenly along a metal wire. For isolated silver bow-tie antennae, the plasmonic resonance blue shifts as the two triangular silver islands are spaced further apart [28]. For the samples prepared in the present work, modeled results predict a similar trend: as the elliptical long axis increases in length, the triangular features become further apart and a blue shift in the low frequency plasmonic feature is seen (see Supplementary Information 3) [27].

As with the fabrication of wire gratings using AR-NSL, or any method for that matter, the infrared response of the elliptical nanoaperture films is strongly polarization sensitive. Since the conductivity along the ellipse long axis is maintained in the form of linear rows of silver that is dotted with bow-tie-like features, the optical transmission of light polarized along the elliptical long axis (90° in Fig. 1) is reduced. When the polarization is rotated by 90° (to 0° in Fig. 1) and is perpendicular to the ellipse long axis, transmission through the films is maintained, per standard grating theory (see Fig. 4).

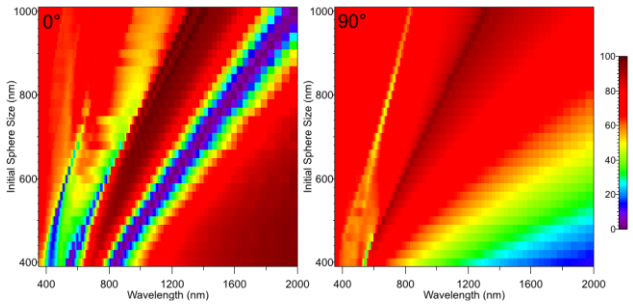

Figure 4 Calculated percent transmission through a 50 nm thick silver film on glass as a function of increasing hexagonal spacing of an array of elliptical apertures showing how the two optical features scale with pitch and incident polarization. The aperture dimensions are defined as 150 nm less than the hexagonal spacing for the short axis (i.e. by a reduction in diameter of 150 nm by etching), and 20 nm longer than the hexagonal spacing for the long axis.

In Fig. 3, the optical transmission through as-produced silver aperture films (Fig. 3a) is compared to modeled spectra calculated using the freely available MIT Electromagnetic Equation Propagation (MEEP) software (Fig. 3b) [29]. As this data and many publications demonstrate, finite-difference time-domain calculations provide an accurate prediction of the optical transmission through nanoaperture films in silver [30]. To demonstrate the usefulness of simple to produce elliptical apertures for polarization-sensitive application ranging from visible applications such as HD displays or fiber optic communication (where the U-Band is defined as ending at 1675 nm), the effect of changing the inter-aperture spacing from 400 nm to 1000 nm is shown in Fig. 4. For any given inter-aperture spacing, a similar tunability in plasmonic resonance is expected to the tunability seen for 438 nm spheres. For the calculations in Fig. 4, the short elliptical axis is defined as 150 nm less than the hexagonal period, while the long axis is defined as 20 nm longer than the hexagonal period. The optical transmission spectra, at both zero and 90-degree polarization, as a function of aperture size and periodicity, are shown in Fig. 4. It is clear from the modeled data that simple to produce structures, in a hexagonal pattern, with sizes ranging from 400 nm to 1000 nm diameter, can be used to produce polarization sensitive plasmonic films in silver. This simple approach is expected to have even better defined spectral features if apertures are produced for example in a manner similar to Cataldo et al [22, 31].

In conclusion, simple to prepare, large-area arrays of plasmonic apertures with tunable and polarization sensitive optical properties are demonstrated. Using angle-dependent silver deposition through nanosphere lithography masks, plasmonic resonances are shown to change nearly 300 nm with increasing aperture ellipticity for the case of 438 nm aperture spacing. The applicability of such a system to visible and near infrared applications is demonstrated with optical modeling using the well-known MEEP software, showing polarization sensitive plasmonic properties from 550 nm to 1700 nm by simply changing the hexagonal spacing.

Acknowledgements AJM acknowledges the financial support of the Alexander von Humboldt-Stiftung and technical discussions with E. Pfitzner of FU Berlin and T. Sun of Boston College regarding MEEP. VO acknowledges financial support of the Deutscher Akademischer Austauschdienst (DAAD).

References

[1] K. Kneipp, Y. Wang, H. Kneipp, L. T. Perelman, I. Itzkan, R. Dasari and M. S. Feld, Phys Rev Lett **78**, 1667-1670 (1997).
[2] M. Moskovits, J Raman Spectrosc **36**, 485-496 (2005).
[3] J. N. Anker, W. P. Hall, O. Lyandres, N. C. Shah, J. Zhao, and R. P. Van Duyne, Nat Mater **7**, 442-453 (2008).
[4] J. Homola, S. S. Yee, and G. Gauglitz, Sens Actuat B-Chem **54**, 3-15 (1999).
[5] A. D. McFarland and R. P. Van Duyne, Nano lett, **3**, 1057-1062, (2003).
[6] V. E. Ferry, J. N. Munday, and H. A. Atwater, Adv Mater **22**, 4794-4808 (2010).
[7] A. J. Morfa, K. L. Rowlen, T. H. Reilly, M. J. Romero, and J. van de Lagemaat, Appl Phys Lett **92**, 013504 (2008).
[8] S. Pillai and M. A. Green, Solar Energy Materials and Solar Cells **94**, 1481-1486 (2010).
[9] M. Westphalen, U. Kreibig, J. Rostalski, H. Luth, and D. Meissner, Sol Energ Mat Sol C **61**, 97-105 (2000).
[10] C. Genet and T. W. Ebbesen, Nature **445**, 39-46 (2007).
[11] J. R. DiMaio and J. Ballato, Opt Express **14**, 2380-2384 (2006).
[12] X. L. Zhu, S. S. Xiao, L. Shi, X. H. Liu, J. Zi, O. Hansen, et al., Opt Express **20**, 5237-5242 (2012).
[13] D. L. Jeanmaire and R. P. Vanduyne, J Electroanal Chem **84**, 1-20 (1977).

[14] T. H. Reilly, S. H. Chang, J. D. Corbman, G. C. Schatz, and K. L. Rowlen, J Phys Chem C **111**, 1689-1694 (2007).
[15] C. L. Haynes and R. P. Van Duyne, J Phys Chem B **107**, 7426-7433 (2003).
[16] W. E. Doering and S. M. Nie, J Phys Chem B **106**, 311-317 (2002).
[17] T. Zhu, H. Z. Yu, J. Wang, Y. Q. Wang, S. M. Cai, and Z. F. Liu, Chem Phys Lett **265**, 334-340 (1997).
[18] P. Patoka and M. Giersig, J Mater Chem **21**, 16783-16796 (2011).
[19] J. C. Hulteen and R. P. Vanduyne, J Vac Sci Technol A **13**, 1553-1558 (1995).
[20] J. Yu, C. Geng, L. Zheng, Z. H. Ma, T. Y. Tan, X. Q. Wang, et al., Langmuir **28**, 12681-12689 (2012).
[21] P. Patoka, T. Y. Sun, M. Giersig, Z. F. Ren, and K. Kempa, Adv Mater **24**, 3042-3045 (2012).
[22] J. Zhao, B. Frank, S. Burger, and H. Giessen, Acs Nano **5**, 9009-9016 (2011).
[23] C. L. Haynes, A. D. McFarland, M. T. Smith, J. C. Hulteen, and R. P. Van Duyne, J Phys Chem B **106**, 1898-1902 (2002).
[24] E. Altewischer, M. P. van Exter, and J. P. Woerdman, J Opt Soc Am B **22**, 1731-1736 (2005).
[25] K. J. K. Koerkamp, S. Enoch, F. B. Segerink, N. F. van Hulst, and L. Kuipers, Phys Rev Lett **92**, 183901 (2004).
[26] B. Sepulveda, Y. Alaverdyan, J. Alegret, M. Kall, and P. Johansson, Opt Express **16**, 5609-5616 (2008).
[27] See, "supplemental material at [URL will be inserted by Wiley] for details of sample size, aperture ellipticity and orientation.."
[28] D. P. Fromm, A. Sundaramurthy, P. J. Schuck, G. Kino, and W. E. Moerner, Nano lett **4**, 957-961 (2004).
[29] A. F. Oskooi, D. Roundy, M. Ibanescu, P. Bermel, J. D. Joannopoulos, and S. G. Johnson, Comput Phys Commun **181**, 687-702 (2010).
[30] A. Taflove and S. C. Hagness, Computational Electrodynamics: The Finite-Difference Time-Domain Method. (Artech House, Norwood, 2000).
[31] S. Cataldo, J. Zhao, F. Neubrech, B. Frank, C. J. Zhang, P. V. Braun and H. Giessen, Acs Nano **6**, 979-985 (2012).